Optical Diagnostic Imaging of Multi-Rocket Plume-Induced Base Flow Environments

Manish Mehta[1] and Darrell E. Gaddy[2]
NASA Marshall Space Flight Center, Huntsville, Alabama, 35812

Paul M. Danehy[3], and Jennifer A. Inman[4]
NASA Langley Research Center, Hampton, Virginia, 23666

and

Ron Parker[5] and Aaron T. Dufrene[6]
CUBRC Inc., Buffalo, New York, 14225

Non-intrusive optical diagnostic imaging was used for the first time to visualize multi-rocket plume-induced reacting base flows to simulate launch vehicle ascent from sea-level to 250,000 ft. In particular, planar laser induced florescence (PLIF) and infrared (IR) imaging were implemented for the first time to visualize and quantify base flow and rocket plume environments from sub-scale, short-duration propulsion models within a shock tunnel facility. This report discusses the successful imaging diagnostic methods for capturing base flow features and dynamics as a function of altitude. Important base flow and plume features were captured with PLIF and IR diagnostics to develop a conceptual base flow physics model. This imaging data specifically provides insight into the Space Launch System vehicle core-stage and Exploration Upper Stage base environments and further validates short-duration ground test techniques and computational modeling.

Nomenclature

AoA	=	Angle-of-Attack
CFD	=	Computational Fluid Dynamics
CO_2	=	Carbon Dioxide
DFI	=	Development Flight Instrumentation
EUS	=	Exploration Upper Stage
FOV	=	Field of View
FWHM	=	Full-Width at Half Maximum
GH_2	=	Gaseous hydrogen
GO_2	=	Gaseous oxygen
H_2	=	Hydrogen
He	=	Helium
IR	=	Infrared
BCL	=	Base Heat Shield Centerline
NCL	=	Nozzle Centerline

[1] Aerospace Engineer, Aerothermodynamics, Aerosciences Branch, Member AIAA
[2] Aerospace Engineer, Thermal Analysis Branch, Member AIAA
[3] Senior Technologist, Advanced Measurement and Data Systems Branch, Associate Fellow AIAA
[4] Aerospace Engineer, Advanced Measurement and Data Systems Branch, Member AIAA
[5] Aerospace Engineer, Aerothermal/Aero-optic Evaluation Center, Member AIAA
[6] Aerospace Engineer, Aerothermal/Aero-optic Evaluation Center, Member AIAA

LARC = Langley Research Center
MSFC = Marshall Space Flight Center
MPCV = Multi-Purpose Crew Vehicle
N_2 = Nitrogen
OH = Hydroxyl radical
O/F = Oxidizer to Fuel Ratio
LWIR = Long-wave Infrared
MWIR = Mid-wave Infrared
PLIF = Planar Laser-Induced Fluorescence
RCS = Reaction Control System
P_{lip} = Nozzle lip pressure
P_{inf} = Freestream pressure
SLS = Space Launch System
TPS = Thermal Protection System
UV = Ultra-violet

I. Introduction

Base flows are one of the highest design risks within the launch vehicle aerothermal discipline due to (1) lack of analytical solutions to adequately predict flow behavior and (2) highest heating environments historically observed during launch vehicle ascent. The base region of a launch vehicle has multiple rocket engines clustered to provide the needed thrust (Figure 1). Multiple rocket plumes and plume-freestream air interactions can lead to highly complex and dangerous heating environments. Multi-rocket engine launch vehicles are common and have been used historically in the Shuttle, Saturn V and Saturn IB (shown in Figure 1) vehicles and ones currently in development such as the Space Launch System (SLS). The larger the thrust and higher the number of engines, the greater the complexity and importance in accurately predicting base environments to capture all the high temperature regions. Accurately predicting and visualizing base flow environments are critical for efficiently and safely designing thermal protection systems (TPS). Lack of understanding of launch vehicle base flows have led to a series of catastrophic rocket explosions from the 1960s to modern day as depicted in Table 1. Inadequate predictions of base heating and flow physics have led to the failures of many government and private launch vehicles during ascent (e.g. Polaris, Atlas, N-1, Prospector, etc.). Hot rocket plume-induced base flows can lead to thermal breakdown of multiple components within the vehicle base such as the propulsion systems, gimbal actuators, cabling for avionics and structural hardware. Thermal protection systems are used to protect these components from high heating environments, and their design can be compromised and lead to mission failure due to inadequate predictions. Overly conservative TPS design, which can weigh ~2,000 lbs per inch on the base heat shield and an additional ~3000 lbs for engine close-outs and other supporting brackets for a typical launch vehicle, can lead to a significant reduction in payload mass. For upper stage vehicles, one pound reduction in TPS mass leads to a one pound increase in payload mass. NASA is designing a 9 million pound thrust SLS vehicle with multiple rocket engines and solid rocket motors for humans to explore deep space. As a result, base heating rates and drag will be considerably higher than current launch vehicles and the flow physics needs to be understood for efficient and safe design of the thermal protection system (TPS).

Prior flow visualization of rocket plume-induced base flows conducted were limited. Successful schlieren images were not obtained of the reacting base flows due to the low resulting density gradients.[1] In the 1960s, hydrocarbon rocket engines minimally showed base flow behavior with poor visualization in the visible spectrum.[2] Flow tag markers in the base did show signs of successful visualization, but did not provide any details in the flow structure. No such base flow visualization investigation was conducted for the full-stack (IH-39) or orbiter-only (OH-65) Space Shuttle base heating test programs.[3,4] Geothert, Brewer, Matz and Little visualized base flows with limited success using seeded smoke for non-reacting cold nozzle flow tests.[5-8] Cold nozzle flow approaches could not provide valid gas temperature maps or information on turbulent structures and showed poor visualization in the visible spectrum. Cold nozzle plume-induced base flows significantly deviate in the specific heat ratio, temperature, mass fraction and composition from combustion gases. These gross simplifications have an effect on the shock structure, viscous flow behavior and turbulent eddy scales. The reacting chemistry within the base is also not captured. Computational fluid dynamics (CFD) has limited success in adequately predicting reacting turbulent flows and plume-induced environments due to inadequate turbulence/chemistry models.[2] However, data acquired in hot-fire ground based tests are helping improve computational modeling.

Historically, intrusive pitot and static pressure and thin hot-wire anemometer probes and rakes were used for flow characterization.[6,7] There were many disadvantages with this approach: (a) probes were very thin and many failed during

installation procedures or testing, (b) probes were intrusive and altered the base flow field, (c) poor data quality of gas temperature measurements which showed an uncertainty of +/- 50% of the mean value for the Shuttle (IH-39, OH-65) base heating test programs[3,4], (d) IH-39 temperature probes recorded much lower values than for flight measurements and could not directly determine heat transfer coefficients.[4] As a result, there is currently no published work on adequate reacting rocket plume-induced base flow visualization and characterization and without this technology there are technical gaps in space vehicle thermal design. Flow field visualization and characterization are needed to understand the flow physics, capture peak heating regions not obtained by discrete measurements and assist in providing important context to the surface heat transfer and pressure measurements. Flow visualization for sub-scale ground based tests are critical to accurately predict launch vehicle and spacecraft environments.

The major objective for this study was to determine the feasibility of various novel non-intrusive optical diagnostics to capture complex launch vehicle rocket plume-induced base flow physics in a ground test facility. Such diagnostic imaging can provide confirmation of the hot-fire shock tunnel test technique, and can improve fidelity of predicted environments and computational model validation. Hydroxyl radical – planar laser induced fluorescence (OH-PLIF) and carbon-dioxide seeded infrared (IR) imaging were the optical diagnostics proposed to visualize and characterize base flows of the 2% Space Launch System (SLS) core-stage and 3.2% Exploration Upper Stage (EUS) hot-fire propulsion models at various altitudes that were used in the Technology Innovation Program (TIP) and EUS test programs, respectively. These diagnostics were developed and tested in collaboration with NASA Marshall Space Flight Center (MSFC), NASA Langley Research Center (LaRC) and CUBRC Inc.

The TIP was first proposed to strictly determine the feasibility of acquiring non-intrusive optical imaging data of model rocket plumes and base flows. To reduce cost to the program, the SLS base heating model was used with no modifications as shown in Figure 2. Based on the success of the FY16 TIP program, the ground test technology in conjunction with the optical diagnostic techniques developed during TIP were used for the NASA SLS EUS base heating test program. This test was conducted to determine in-space base environments for the Block1B/EUS vehicle. The EUS vehicle has four RL-10 LOX/LH_2 engines that operate for two 500+ second burns: (1) 100 x 1000 nmi orbit to low earth orbit (LEO) while meeting core-stage disposal constraints and (2) LEO departure burn where it places the stage in heliocentric orbit. These relatively long burn times lead to large heat loads. These loads may necessitate the use of a base thermal protection system, and at the time of the EUS test it was unclear whether the current design (using multi-layer insulation) was adequate. This high fidelity EUS base heating test program was therefore conducted to support EUS Preliminary Design Review (PDR) base design trades and Critical Design Review/Design Analysis Cycle (DAC) 2 environments. The surface measurements and imaging shown in Figure 2 provides data that will inform engine and base heat shield designs. The surface measurement and imaging data provides NASA with a good understanding of the flow physics, maps of all “hot spots” in the vehicle aft section, and improves the fidelity of the test data and ground test technique.

To increase the technology readiness level (TRL) of the short-duration (<100 milliseconds) propulsion ground test technology, this research investigation conducted during the TIP and EUS test programs proposed to address three main areas which historically had deficiencies: (1) visualize launch vehicle base flows due to multi-rocket engine plumes for short-duration testing; (2) obtain high spatial resolution measurements of base gas temperature; (3) confirm scaling laws used for developing plume-induced environments.

Figure 1. Multi-rocket engine launch vehicle base regions: Shuttle Orbiter (top-left); Shuttle (top-right); Saturn 1-B (bottom-left); Saturn V (bottom-right)

Table 1. Launch Vehicle Failures Due to Base Flows

Rocket	Date	Outcome	Cause
JUPITER AM-1A	3/1/57	Failure	Base heating - Control Loss
ATLAS SM-65 A	6/11/57	Failure	Base heating - Control Loss
ATLAS SM-65 A	9/25/57	Failure	Base heating - Control Loss
THOR 114	1/1/58	Failure	Base heating - Control Loss
POLARIS A-1	12/30/58	Failure	Base heating - Control Loss
POLARIS A-1	1/9/59	Failure	Base heating - Control Loss
SATURN I	10/21/61	Concern	Base heating - Base Flow
SATURN IB	2/26/66	Concern	Base heating - Base Flow
SATURN V	11/6/67	Concern	Base heating - Base Flow
N-1 (SOVIET)	2/1/72	Failure	Base Flow - Roll Control
MAXUS (GERMAN)	5/1/91	Failure	Base heating - Control Loss
PROSPECTOR	6/19/91	Failure	Base heating - Control Loss

II. Methodology

A. Infrared (IR) Imaging System

Two types of infrared cameras were used for these test programs: a long-wave infrared (LWIR) camera (FLIR a655sc) and a mid-wave infrared (MWIR) camera (FLIR 8000sc). Figure 2 shows the various imaging diagnostics used to visualize the rocket plumes and base flows at various altitudes. The LWIR camera captured emitting wavelength from 7.5 microns to 14 microns with a resolution of 640 x 240 pixels and frame rate of 100 Hz set to the low temperature sensitivity range. The LWIR camera has an uncooled a Vanadium Oxide microbolometer detector. This detector element changes in resistance due to an increase in radiant temperature. The LWIR camera, the black camera in Figure 2, was placed on the top of the LENS I facility and looked through a germanium window. The MWIR captured wavelengths from 3 to 5 microns with a resolution of 512 x 256 pixels at a frame rate of 180 Hz, with images acquired at multiple temperature ranges. The MWIR camera was placed next to the LWIR camera looking through a zinc selenide window. All cameras were external to the test facility as shown in Figure 2. Low temperature range IR detector sensitivity was chosen to capture all the various flow structures. The MWIR camera has a cooled Indium Antimonide detector. This detector changes the resistivity of the detector element due to IR photons electronic excitations. Cooled detectors have higher sensitivity due to the decrease in internal thermal noise. Both detectors output voltages for each detector element which provides a 2-D image. Both cameras had 41 mm lenses with 15-degree fields of view. The IR imaging and supporting windows were supplied by NASA MSFC's Thermal Analysis and Test Branch (ER43).

B. Planar laser-induced fluorescence (PLIF) Imaging System

The hydroxyl (OH) radical, which is one of the product species for the GH_2-GO_2 combustion process, is used as the fluorescent medium for imaging. This does not require artificial seeding of the combustion gases. OH PLIF uses an ultraviolet laser sheet to interrogate a slice in the flow. This UV light excites the OH molecules, resulting in fluorescence which is detected by an intensified digital camera. Details of the measurement system used in this experiment, as well as the experimental procedure used, can be found in References 9, 10 and 11. One of NASA Langley's two mobile PLIF systems was shipped to CUBRC and installed next to the LENS-I facility. The laser system uses an injection seeded neodymium-doped yttrium aluminum garnet, $Nd:Y_3Al_5O_{12}$ (Nd:YAG), laser to pump a Sirah Cobra Stretch dye laser and Sirah Frequency Conversion Unit (FCU). The dye laser was operated near 567 nm and was frequency doubled to produce about 20 mJ/pulse of UV light used to excite the naturally occurring OH. The resulting laser output, was tuned to excite the strongly fluorescing spectral lines of OH in the strong the strong Q branch bands (where Q denotes a change in rotational quantum number, *J*, equal to zero).The laser was tuned to probe a variety of absorption lines having different temperature sensitivities. The main line probed was at 283.53 nm which probed the Q_1 (8) line which has weak temperature sensitivity (does not vary with temperature over a wide range of high temperatures), so that most variations in the signal intensity could be interpreted qualitatively as OH concentration variations. This transition is referred to as the "mid-J" line below. For some runs the laser was tuned to 283.38 nm and 285.55 nm to excite the Q_2 (6) "low-J" and Q_2 (12) "high-J" lines which were more sensitive at low and high temperature regions of the flow, respectively.

To reach the model, the UV laser beam passed up to the top of the facility where it was formed into a laser sheet using a 150 mm focal length cylindrical lens followed by a 2000 mm focal length, 100 mm diameter spherical lens which was nearly 2 meters from the capsule model installed in the wind tunnel. The distance between the two lenses was adjusted so that the laser sheet would expand to a width of about 100 mm inside the test section. The resulting laser sheet was about 1 mm thick (FWHM) in the measurement region. The same cameras, PIMAX camera shown in brown and DiCAM camera shown in blue (top left image of Figure 2), excitation schemes, etc., were used as in past work. For the TIP test, the PIMAX camera had an *F*/4, *f*=105 mm focal length Nikon lens and a 1" diameter Semrock interference filter that transmitted the OH fluorescence while blocking the laser's wavelength and much of the visible light spectrum. To improve the signal to noise ratio for the EUS tests, an identical but larger (2" diameter) filter was procured, and a faster lens was used (Halle, *F*/2, *f* = 100 mm focal length) which increased the signal intensity by a factor of 4 significantly improving the signal to noise ratio. The fluorescence was imaged onto a gated, intensified CCD at a viewing angle normal to the laser sheet. The camera magnifications were measured from images acquired of a regular pattern of dots of known spacing (known as a *dotcard*), with this dotcard placed in the image plane. The camera FOV was about 200 mm. The images can be obtained at a rate of 10 Hz with flow-stopping time resolution (<1 microsecond). A timing circuit was developed to synchronize the Nd:YAG laser operation and camera with the pulsed facility. The laser sheet forming optics were on a translation stage so that they could be precisely aligned to different planes of the model such as the Body Centerline (BCL) or the Nozzle Centerline (NCL). Finally, a third camera was set up to monitor the energy and spatial profile of the laser sheet. This image viewed the fluorescence resulting from illumination of laser dye dissolved in water by a small fraction of light (~1%) split off of the main laser sheet. The laser-sheet intensity and spatial distribution was measured on a shot-to-shot basis. The PLIF system was provided by NASA Langley's Advanced Measurement and Data Systems Branch (D304).

C. PLIF and IR Flow Visualization Image Processing

Single-shot PLIF images were processed using smoothing routines and by adding false color tables. Images were not corrected for spatial variations in laser sheet intensity because they were not observed to vary with laser intensity because it is believed that the fluorescence was saturated owing to such low operating pressures and high laser fluence. The images were first corrected by subtracting the background noise which was done by subtracting the average intensity from the entire image acquired with the laser operating but no exhaust plume flow. To remove other sources of noise, a 2-D Gaussian filter with one standard deviation was applied to the PLIF images. Thresholding was applied to the image where the peak emission pixel value within the flow domain was the max value used. These images were then converted to MATLAB "jet" color scale. The images were then made into bitmap images or movies for display on TecPlot models. These images were not post-processed for thermometry, but to provide details in the flow structures.

Multiple IR images were acquired during a test run. These cameras acquire infrared radiation emitted by the object and transform it into electrical signals. Images acquired using infrared cameras are converted into visible images by assigning a color to each infrared energy level. The result is a false-color image called a thermogram. Most of the IR images were converted to MATLAB "jet" color scale, but a few images were converted to "iron bow" color scale. To determine surface wall temperatures, the technique of compensation is required in post-processing these images. Radiation is received by the camera from three sources: (1) emission of the target, (2) emission of the surrounding and reflected by the object, and (3) the emission of the atmosphere. The reflection component was minimized by applying flat black paint with known emissivity to

the model and covering the tunnel wall with black cloth. The last two components are subtracted from the total infrared emission to obtain the thermogram with surface wall temperature values. It should be noted that plume temperatures were not obtained from these post-processed IR images due to the difficulty in determining the emissivity of the plumes.

III. Results

A. FY16 Technology Innovation Program (TIP)

The FY16 TIP GH_2-GO_2 SLS core-stage propulsion model had four 2% scale RS-25 nozzles with an expansion ratio of 70 on a truncated SLS core-stage base as shown in Figure 2. There was a large sting incorporated within the LENS I test facility. No freestream flow was initiated for these tests and the facility was used as a vacuum chamber. Suppressing the freestream flow allowed for many more tunnel runs to be obtained per day, resulting in faster improvements in the test techniques while still investigating relevant flow conditions. The base heat shield and the four rocket nozzles were painted a flat black with known emissivity to estimate surface temperatures from IR imaging. The rocket nozzle was made of refractory metals to prevent thermal shock degradation and to meet nozzle boundary layer specific enthalpy requirements. In addition, the model was painted to prevent artificial light scattering to minimize reflections that corrupt IR and PLIF data. A large black cloth was also installed to cover the metallic tunnel walls. As can be seen in Figure 2, thin-film heat transfer gauges and piezo-resistive pressure gauges were installed on the base heat shield to measure heating and pressure environments. Piezo-electric pressure gauges were installed within the engine to determine performance. These propulsion models were derived from the SLS base heating test program and this test program.

There are some differences in the performance of these model engines when scaled to flight. As observed in Table 2, the chamber pressure for these model engines were smaller than the flight RS-25 engine performance values. It can also be seen that the model engine O/F ratio was higher than the flight engine performance to increase the OH concentration within base flows. Three different OH lines with different temperature sensitivities were excited using PLIF, herein called mid-J, low-J and high-J to obtain base gas temperature measurements to be reported elsewhere. In some cases, carbon-dioxide was bled into the combustion chamber to improve the infrared imaging sensitivity. Carbon dioxide is a strong emitter within 3 to 5 microns and theoretically should improve IR base flow visualization. Except for the first hot-fire run, IR and PLIF were both on-line for each test.

Figure 3 shows the chamber pressure (a), O/F ratio (b), base pressure (c) and base heat transfer rates (d) as a function of test run time at two different freestream pressure settings. Most of the engine burn times for the TIP test program were on the order of 100 milliseconds (msec) to minimize nozzle throat erosion. Nozzle throat erosion was not observed for any of the TIP tests. The engine performance and external measurements are relatively steady during the engine burn. Internal GH_2-GO_2 rocket engine data (Figure 3) and base surface heat transfer measurements (Figure 3) provide critical information to further understand the flow physics and provide an anchor to the imaging data. The model rocket engine operated at a chamber pressure of ~500 psia and oxidizer to fuel ratio (O/F) of ~6.7. In mid-September 2016, a total of 23 hot-fire tests were completed within LENS I test facility with no tunnel flow and target test section pressures between 93 mTorr and 129,287 mTorr. This translates to equivalent altitudes between sea-level and 170,000 feet. Figure 3 also shows the drastic difference in base external environments between sea-level and high-altitude regimes. It can be seen that the convective heat flux at high altitude is two orders of magnitude larger than at sea-level with chamber pressure and O/F ratio relatively the same for both test runs. Not shown as readily, but base pressure differential (base pressure subtracted by the freestream pressure) is much larger as well. Figure 4 is contour plot which shows high base heating is clustered around the central region of the base for the high altitude regime. It can be seen that low uniform base heat flux is observed during the sea-level regime. This change in distribution and magnitude between the two altitude regimes is further investigated through flow visualization techniques. Through measurements and flow visualization, a conceptual base flow physics model will be attempted.

Table 2. TIP Test Matrix

Run	Test	Pressure (mTorr)	Diagnostics	Temp Line	Pc (psia)	O/F	Notes
Run 01	TIP	120	IR	Mid J	447	5.9	BCL
Run 02	TIP	120	IR/PLIF	Mid J	441	6.1	NCL
Run 04	TIP	100	IR/PLIF	Mid J	525	6.8	BCL
Run 05	TIP	96	IR/PLIF	Mid J	526	7.2	BCL
Run 06	TIP	93	IR/PLIF	Mid J	536	6.84	BCL, CO2 seed (8 psi)
Run 07	TIP	93	IR/PLIF	Mid J	522	6.77	NCL, CO2 seed (6 psi)
Run 08	TIP	98	IR/PLIF	Mid J	455	6.6	BCL
Run 09	TIP	97	IR/PLIF	Mid J	493	533	BCL
Run 10	TIP	97	IR/PLIF	Mid J	498	6.8	NCL
Run 11	TIP	96	IR/PLIF	Mid J	540	6.7	NCL
Run 12	TIP	96	IR/PLIF	Hi J	531	6.7	BCL
Run 13	TIP	97	IR/PLIF	Hi J	524	6.8	BCL
Run 14	TIP	96	IR/PLIF	Hi J	523	6.7	BCL, Bad Run
Run 15	TIP	96	IR/PLIF	Hi J	519	6.8	BCL, Bad Ruun
Run 16	TIP	96	IR/PLIF	Lo J	528	6.8	BCL
Run 17	TIP	96	IR/PLIF	Lo J	515	6.8	BCL
Run 18	TIP	95	IR/PLIF	Lo J	516	6.7	BCL, CO2 seed (60 psi)
Run 19	TIP	259	IR/PLIF	Mid J	380	6.6	BCL
Run 20	TIP	259	IR/PLIF	Mid J	510	6.7	BCL
Run 21	TIP	602	IR/PLIF	Mid J	524	6.8	BCL
Run 22	TIP	25858	IR/PLIF	Mid J	505	6.7	BCL
Run 23	TIP	129287	IR/PLIF	Mid J	482	6.8	BCL

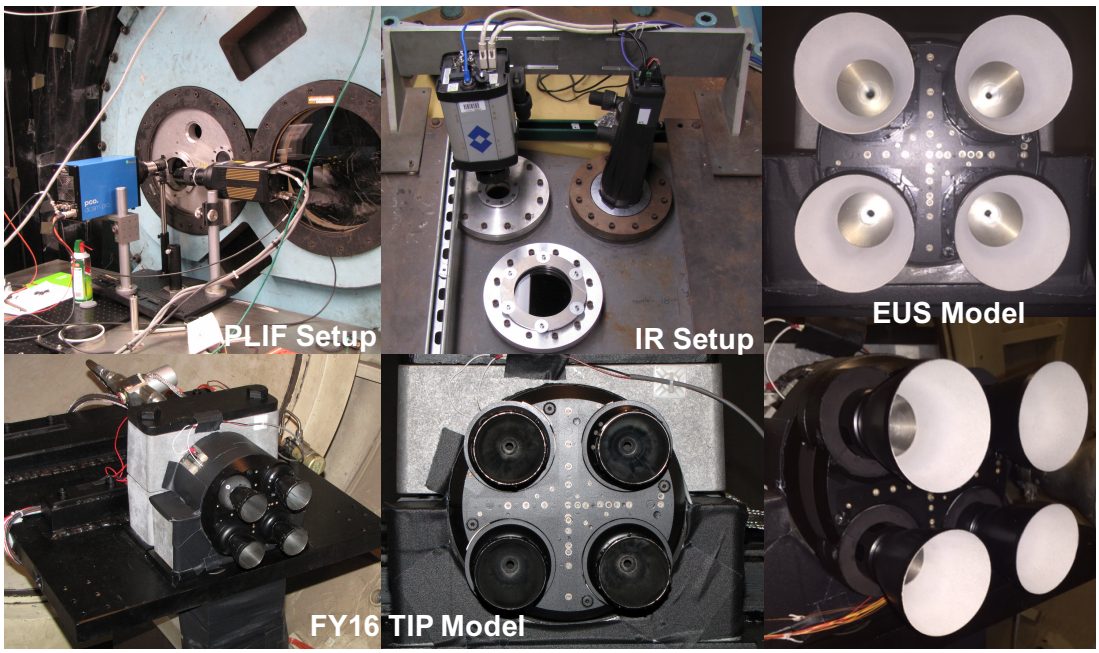

Figure 2. Optical imaging instrumentation, TIP and EUS propulsion models.

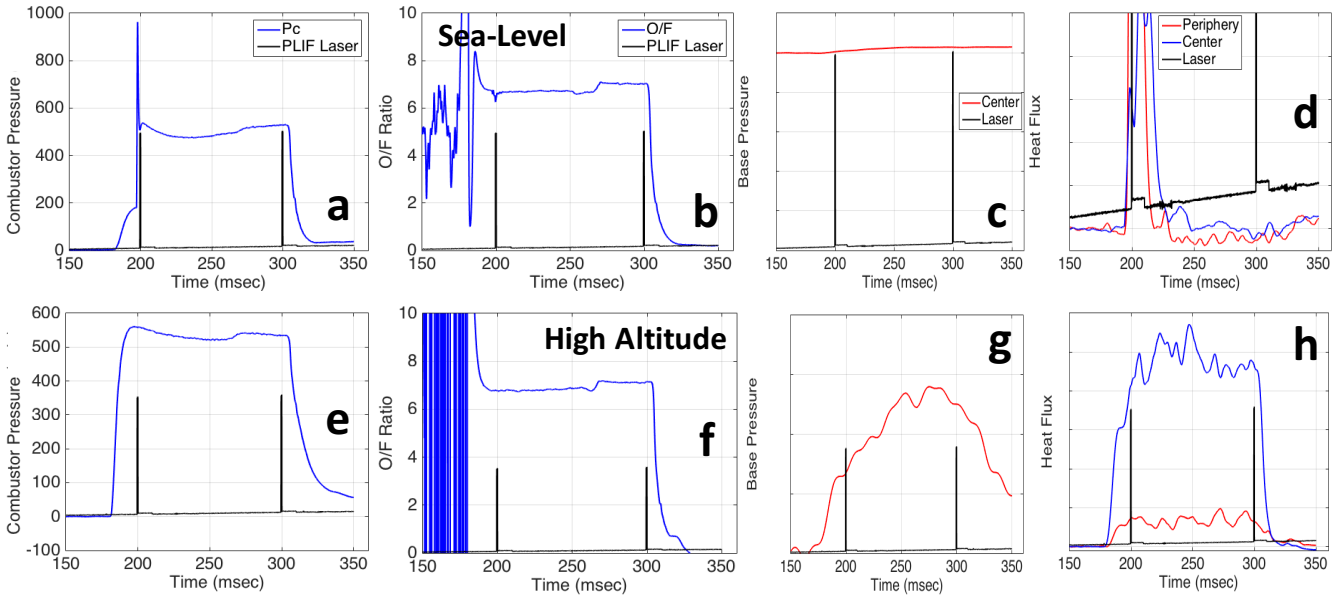

Figure 3. Parameter – time traces for sea-level (Run 23) and high-altitude (Run 4) conditions of a full rocket engine burn.

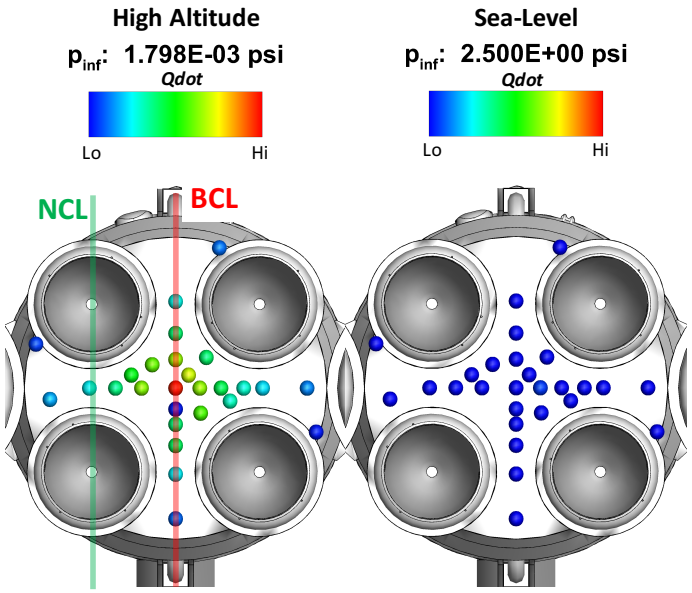

Figure 4. Base heat flux contour test data for high altitude (left) and sea level (right) test conditions

Through this FY16 TIP, non-intrusive optical diagnostics were used for the first time to visualize and characterize the behavior of reacting turbulent flows within a multi-engine configuration launch vehicle base. OH-PLIF imaging, IR imaging and tunable diode laser absorption spectroscopy (TDLAS)[4] successfully captured the turbulent reacting base flows, rocket plumes and base gas temperatures, respectively.

IR imaging captured the inviscid flow features due to the rocket plume structure and plume-plume interactions (e.g. Mach disc, regular shock reflection, reflected shocks, core plume, etc.) at various altitudes simulated during the TIP test program. IR imaging of high altitude and sea-level freestream test conditions are shown in Figures 5 and 6. At high altitudes, reflected shocks and wakes are observed between the two RS-25 nozzles and at sea-level conditions a characteristic Mach disc is observed within the plume downstream of the nozzle exit and the reflected shocks disappear. Regular shock reflections of the four plumes are also observed through IR imaging as shown in Figures 5 and 6. Plume dynamics has a

strong function on base flow behavior. Mid-wave infrared (MWIR) focused in the near-field rocket plumes and within the base region of the test article. Long-wave infrared (LWIR) focused on the far-field plume. Figure 6 provides the quantitative surface temperature of the nozzles and test article during the engine burn along with the characteristic plume features described above. This is the first time that IR imaging focused in the near-field and far-field flow domain simultaneously to provide important context to base flows and accurately provided surface temperatures. Seeding the combustion chamber with a few percent of CO_2, a strong IR emitter, did not prove successful in viewing the base gas flow field due to low optical density and some of the carbon-dioxide disassociation to carbon monoxide. All IR images were processed by MSFC Propulsion Thermal Analysis Branch (ER43) and the Aerosciences Branch (EV33).

The OH-PLIF 2D laser sheet focused on two regions (Figure 4): (a) the base heat shield centerline (BCL) and the (b) nozzle centerline (NCL). OH-PLIF BCL images successfully captured the complex base flow field structures and the altitude-dependent dynamics during a simulated launch vehicle ascent, which contributes to one of the highest vehicle heating environments. High OH emissions correlates to high OH concentration. These images show high emission in the following regions: (a) near the base heat shield, (b) between the exit of two RS-25 nozzles and (c) further downstream from the nozzle exit plane. It can also be seen that emission gradually decreases from between the nozzles near the exit plane toward the base heat shield. This then sees a discontinuous jump in emission correlating to a stagnation shock. As a result, the OH-PLIF imaging showed that for the SLS core-only configuration at altitudes greater than 150,000 feet, a reverse expanding jet results in a stagnation shock upstream of the base, leading to high heating and pressure distributions as shown in Figures 4 and 7. It can also be seen from the OH-PLIF image (Figure 7) that high OH emission is observed in a semi-circular region slightly downstream of the nozzle exit plane. Directly downstream of the nozzle exit plane along the BCL plane, low emission (lower density, cooler gas temperature) regions are observed. Stagnation shock – RS-25 nozzle impingement is observed which can potentially augment heating by a factor of ~10.

The OH-PLIF NCL images captures the hot RS-25 nozzle boundary layer which recirculates within the base[7] and leads to heating observed in Figure 8. The cooler core nozzle flow is also observed. Figure 9 shows the significant base flow field changes between high altitude and sea-level conditions with fixed engine thrust due to base flow recirculation (Figure 9, left) and freestream-induced aspiration (Figure 9, right). These significant base flow structure changes correspond well with the rocket plume structure changes as observed through IR imaging in Figures 5 and 6. The synthesis of IR and OH-PLIF imaging provides a good understanding of the flow physics as will be explored. As can be seen in Figures 7 and 8, good agreement is observed between CFD solutions and the PLIF test data for both the base region and the near-field plumes. All PLIF images shown were targeted for a temperature-insensitive OH excitation wavelength which make it ideal for flow visualization, but high and low temperature-sensitive OH wavelengths were also targeted to obtain a quantitative temperature map of the base region (not shown in this paper). Through first principle assumptions and further post-processing of the images, the goal is to quantify the stagnation shock strength and base flow and nozzle boundary layer temperature fields which are important parameters for base heating and ground test scaling methodologies.

Figure 10 shows the 4-engine base flow physics model[2] at high-altitude regime developed from PLIF and IR imaging and surface measurements. At high altitudes, the freestream pressure is much less than the nozzle exit pressure which leads to highly underexpanded plumes with a large P_{lip}/P_{inf} ~1500. This causes the rocket plumes to expand and interact when in close proximity to each other as observed in the 4-engine case. The two rocket plume shock boundaries interact, resulting in an Edney shock-shock Type I interaction to form wedge-shaped reflected shocks between the pair of nozzles as observed in Figures 5 and 6. There are four reflected shocks that form at the base of the TIP propulsion model within this altitude regime. Within the oblique reflected shocks, the static pressure and temperature increase is captured by IR imaging. These large pressure gradients across the reflected shocks divert the low kinetic energy nozzle boundary layer flow from each nozzle towards the base heat shield as captured by the PLIF images. This supersonic reverse jet expands towards the base heat shield as observed due to a steady drop in static temperature (Figure 6). This supersonic reverse jet forms a strong normal stagnation shock upstream of the heat shield which shows a considerable jump in static flow temperature (emission) within the central region of the base. The flow stagnates and then accelerates radially outward along the base heat shield and is referred to a wall jet. This normal plate shock disc is bounded by interacting with the base of the rocket nozzles which leads to shock impingement on the base of the nozzles. Assessment of this shock heating is currently proceeding and its impact to nozzle external environments will be assessed. The reflected shocks can have clocking unsteadiness due to instantaneous exit pressure variations between the four nozzles which can lead to unsteadiness in the reverse jet as schematically shown in Figure 10.

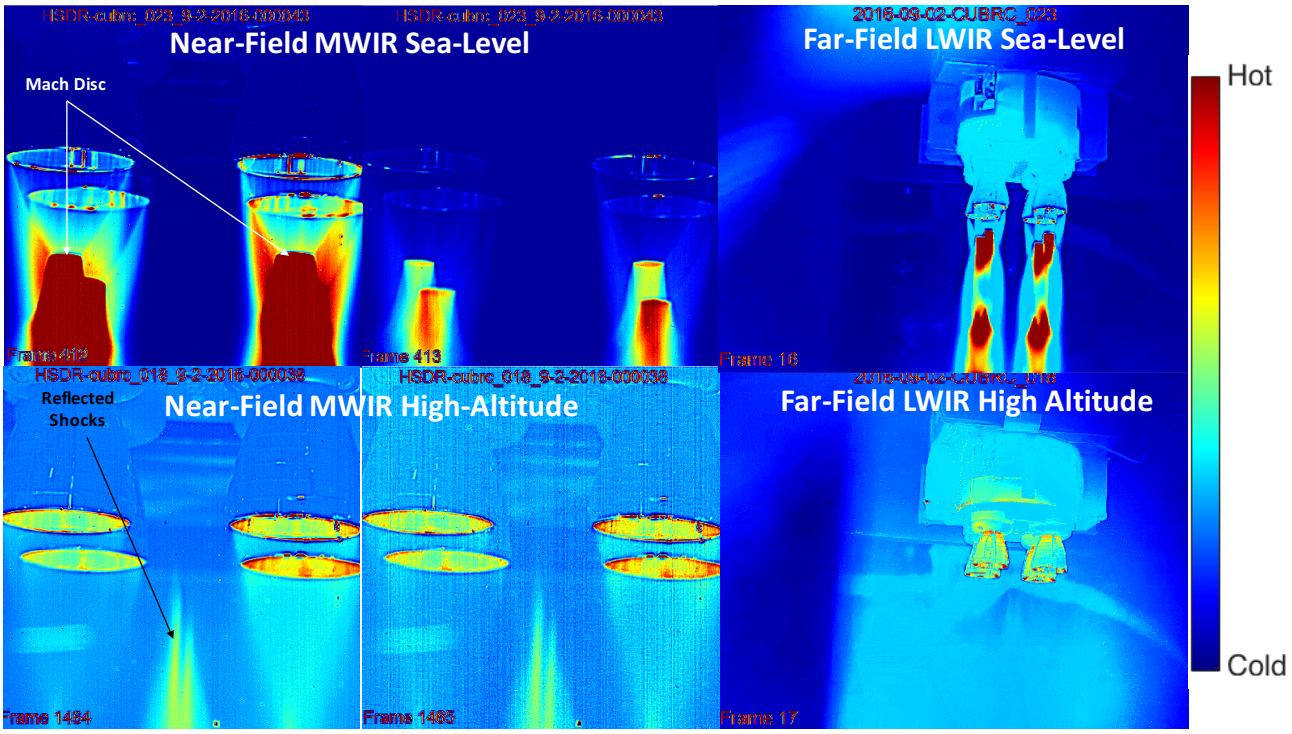

Figure 5. IR imaging captured rocket plume flow structures of sea-level (Run 23) and high-altitude (Run 4)

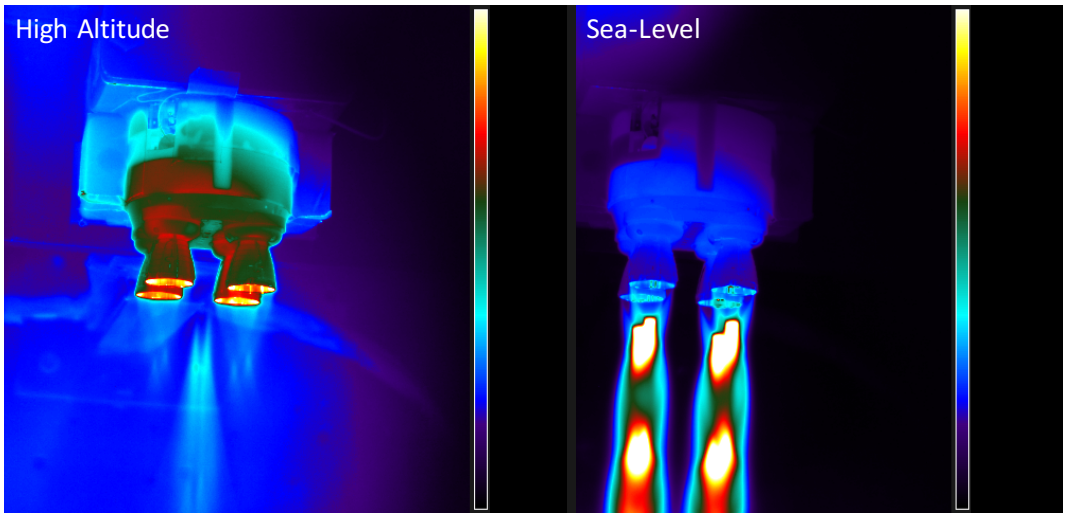

Figure 6. LWIR imaging captured launch vehicle test model base and nozzle surface wall temperatures at sea-level (Run 23) and high-altitude (Run 4) conditions

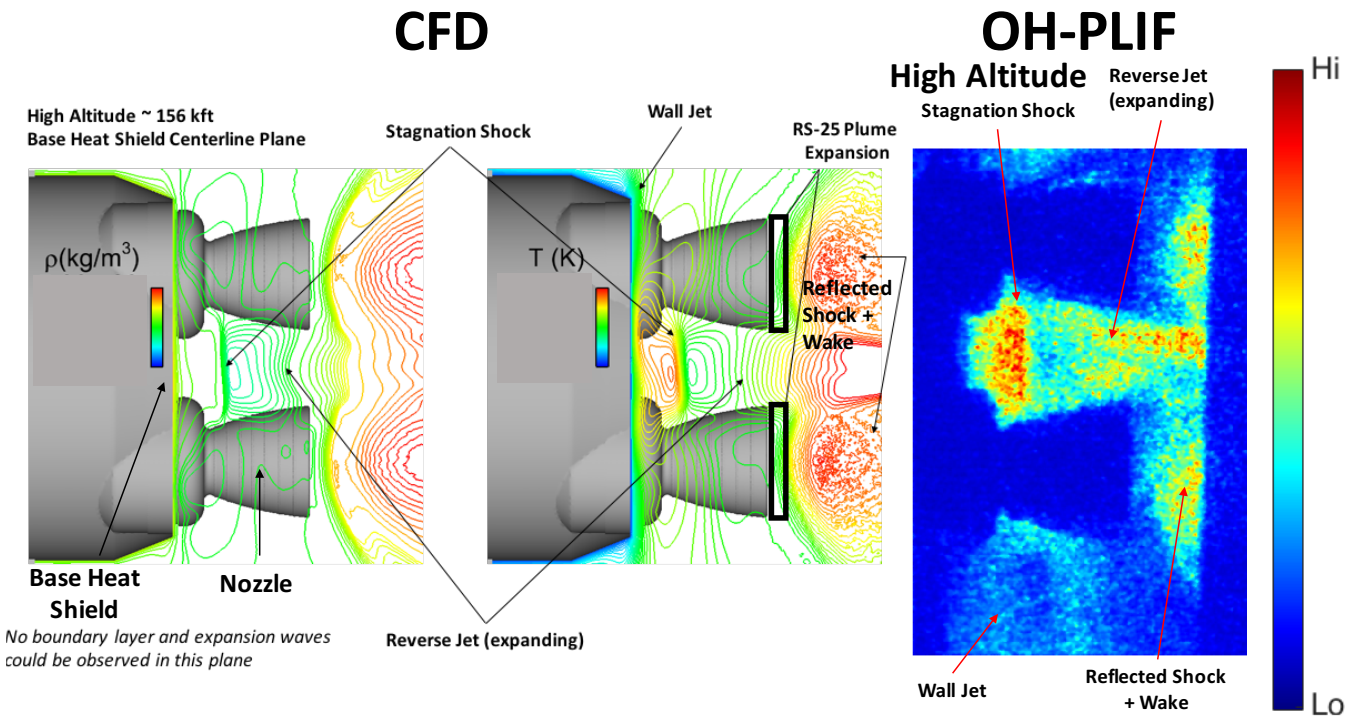

Figure 7. OH-PLIF BCL imaging (Run 6) and CFD calculations of base flow environments

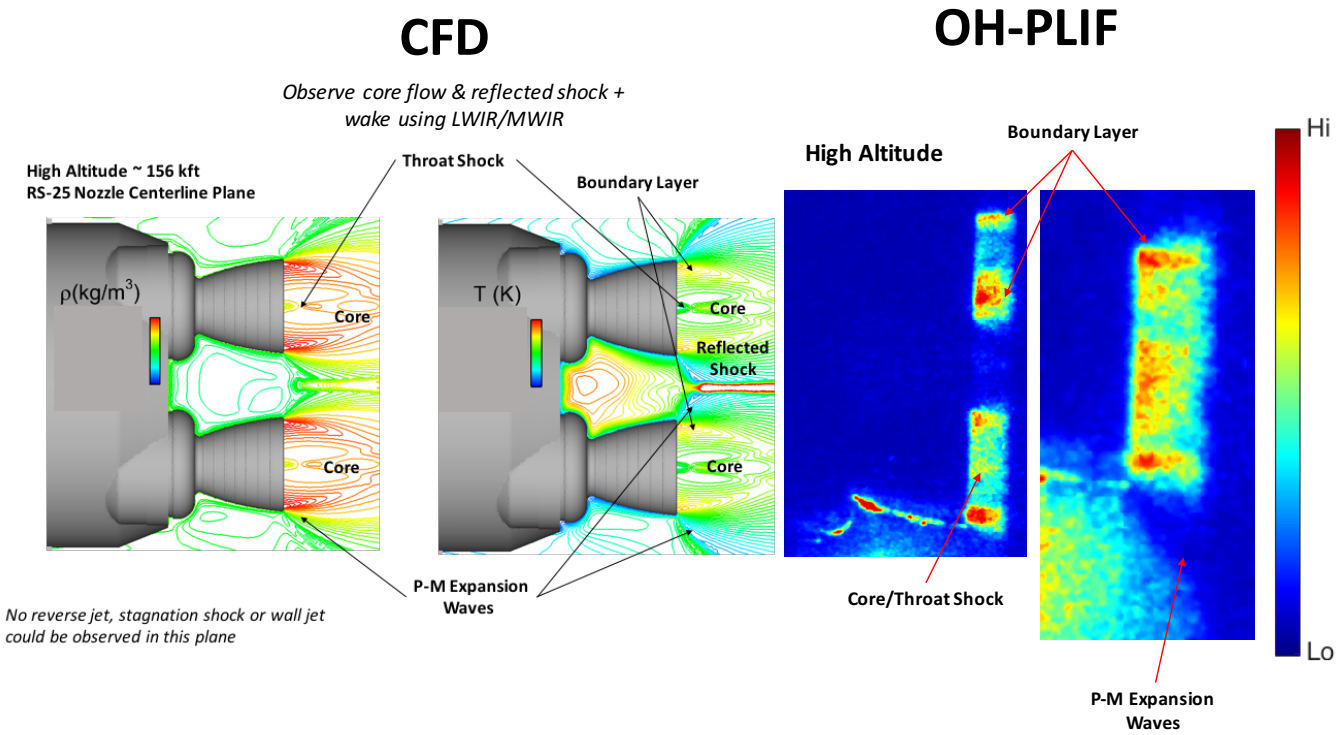

Figure 8. OH-PLIF NCL imaging (Run 11) and CFD calculations of plume environments

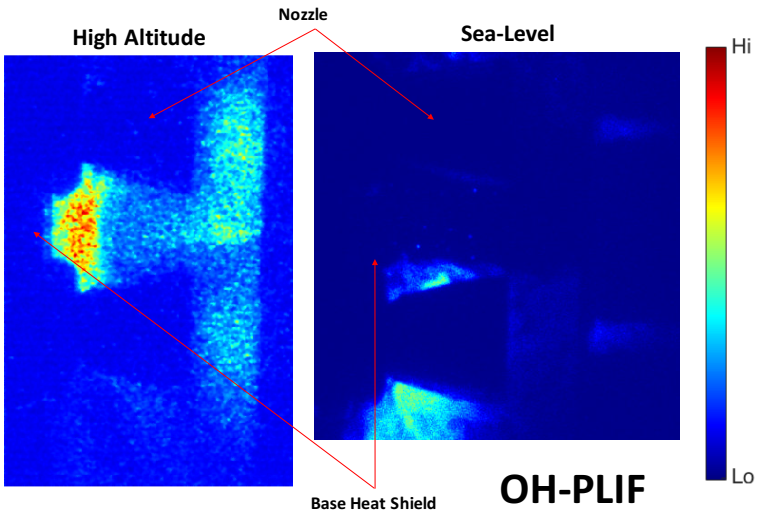

Figure 9. OH-PLIF BCL imaging of base flow environments at high altitude (TIP Run 4) and sea-level (TIP Run 23) conditions

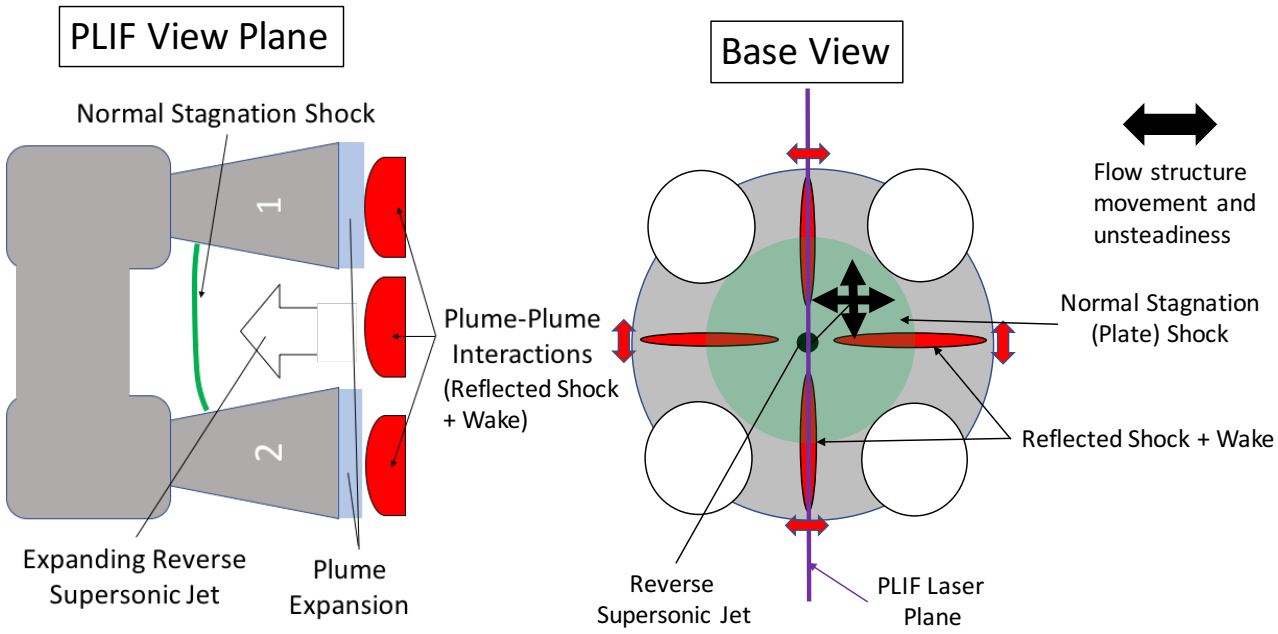

Figure 10. Four-engine base flow physics model[2]

B. EUS Base Heating Test Program

The EUS GO_2 –GH_2 propulsion model had four 3.2% scale RL10 nozzles with an expansion ratio of ~220 on a truncated EUS base as shown in Figure 2. There was a large sting incorporated within the LENS I test facility. No freestream flow was initiated for these tests and the facility was used as a vacuum chamber. The EUS base heat shield was the same as the TIP propulsion model, but the four rocket nozzles were significantly different in inner and outer nozzle contours and nozzle materials and the engine close-outs had different outer mold lines (OML). The RL10 nozzle extension is coated with ceramic (as shown in white in Figure 2) to more closely simulate the boundary layer specific enthalpy due to the flight carbon-phenolic extension. The flight nozzle extension wall temperatures will reach high values due to this portion of the nozzle not being actively cooled and being an effective ablator. Some of the energy will radiate away and slightly reduce the wall temperature. The model was painted also to prevent artificial light scattering to minimize reflections that can disrupt

diagnostic data. A large black cloth was also installed to cover the metallic tunnel walls and floor. As can be seen in Figure 2, thin-film heat transfer gauges and piezo-resistive pressure gauges were installed on the base heat shield to measure heating environments. Piezo-electric pressure gauges were installed within the engine to determine performance.

There were some differences in the performance between the EUS and TIP model propulsion systems. As observed in Table 3, it can be seen that the chamber pressure for these model engines measured were on the order of ~600 psia with an O/F ratio of ~6. Another big difference is the LENS I vacuum chamber operated at less than 20 mTorr which corresponds to altitudes greater than 200 kft. This was an order of magnitude less than the operating test section pressure for the TIP test. The three different OH temperature lines were again excited using PLIF, (so called mid-J, low-J and high-J) to obtain base gas thermometry. In some cases, the engine experienced hard starts mainly due to issues with the glow plug igniter. All tests were performed using the BCL PLIF plane. No seeding of flow within model combustor was conducted for this test to adequately match RL10 flight performance. Except for the first 6 hot-fire runs and Run 17, IR and PLIF diagnostics were both on-line for each test.

Table 3. EUS Test Matrix

Run	Test	Pressure (mTorr)	Diagnostics	Temp Line	Pc (psia)	O/F	Notes
Run 01	EUS	9	IR		456	5.90	
Run 02	EUS	11	IR		640	6.00	
Run 03	EUS	11	IR		618	5.80	
Run 04	EUS	11	IR		603	5.90	
Run 06	EUS	12	IR		617	5.90	
Run 08	EUS	11	IR		609	5.90	
Run 10	EUS	12	IR/PLIF	Mid J	411	6.14	
Run 11	EUS	10	IR/PLIF	Mid J	560	5.77	BCL, Early hard start
Run 17	EUS	16	IR		819	5.80	BCL, Clean start
Run 18	EUS	16	IR/PLIF	Mid J	798	5.80	BCL, Early hard start
Run 19	EUS	3620	IR/PLIF	Mid J	602	5.80	BCL, New glow plug
Run 20	EUS	13	IR/PLIF	Mid J	125	6.19	PLIF did not capture combustion
Run 21	EUS	17	IR/PLIF	Mid J	585	5.52	BCL
Run 22	EUS	18	IR/PLIF	Mid J	607	5.78	BCL
Run 23	EUS	17	IR/PLIF	Hi J	604	5.67	BCL, New glow plug
Run 24	EUS	18	IR/PLIF	Hi J	589	5.82	BCL
Run 39	EUS	15	IR/PLIF	Lo J	521	5.82	BCL Early hard start

Figure 10 shows MWIR images of the model RL10 engine start-up time-sequence for altitudes of 240 kft (18 mTorr) and 118 kft (3620 mTorr) conditions. The characteristic wedge-shaped reflected shocks and associated wake is observed for the high altitude case, but is not observed for the lower altitude condition. The expansion ratio of these nozzles were approximately 220 (a factor of 3 times greater than the RS-25 engine nozzles) which results in plume-plume interactions at much higher altitudes than observed for the SLS core-stage. It can be seen from Figure 10 that the reflected shock structure begins to form about 11 msec from ignition and the apex of the reflected shock is axially located near the nozzle exit plane. Figure 11 shows the comparisons of the RL10 plumes between CFD solutions and MWIR test data. It should be noted that the MWIR emission data is a spatially and temporally averaged image where the CFD solutions are mean steady-state solutions over discrete planes as shown in the figures. The location, length and width of the reflected shocks between CFD and imaging data show good agreement. Due to low density cold core in highly underexpanded rocket plumes, the emission is not high enough to be detected by the IR cameras.

It can be seen from OH-PLIF imaging (Figure 12) that a strong concave stagnation shock (high emission region) is observed aft of the EUS base heat shield due to the expanding supersonic reverse jet, as seen for the high-altitude SLS core-stage vehicle base during the TIP test program. The reverse jet results from the reflected shocks between the RL10 nozzles due to plume-plume interactions as observed from the LWIR and based on the 4-engine base flow physics model. Since these PLIF images are taken at a time-scale of 0.001 msec and the plane thickness is 1 mm, reverse jet unsteadiness can be observed. The reverse jet can be seen moving laterally in and out of the PLIF plane and is corroborated with CFD simulations. Hence, the start of the reverse jet can show high and low temperature contours from run to run with initial similar conditions, but the standoff distance and diameter of the stagnation shock is observed to be fixed for all test runs above 220 kft. This implies that the shock strength is fixed and the reverse jet flow is within the choked regime. The strong stagnation shock (high OH emission corresponding to a strong density change) leads to a large temperature jump and high heating rates, an order of magnitude larger than previous predictions. This is under the assumption that the line is temperature independent and composition is fixed. Along the BCL plane downstream of the nozzle exit, it can be seen that the static temperature contours are low due to the plume expansion and then increase further downstream from the exit as observed for the SLS core-stage TIP test. This increase in static temperature is due to the formation of reflected shocks by plume-plume interactions with the nozzles outside of the PLIF BCL plane (not shown). The characteristic wall jet along the base heat shield can be observed. Good agreement in plate shock standoff distance and diameter and qualitative temperature

distribution within the shock layer are observed between CFD and PLIF data. Through IR and OH-PLIF imaging and in conjunction with surface measurements (not shown), the base flow physics model for the EUS configuration is confirmed.

Figure 13 shows the steady-state CFD solution at 250 kft of the EUS flight configuration. It can be seen that there is good agreement between flight and test CFD and ground test data in the various flow structure locations and geometries and qualitative static gas temperature distribution within the reverse jet and stagnation shock layer. IR and PLIF diagnostics in conjunction with CFD suggests that the ground test technique is accurately simulating the appropriate general base flow physics with flight. This leads to further confidence in the test-derived base flow environment predictions. However, predicted base environments with development flight instrumentation (DFI) data is necessary to adequately confirm this ground test technique. If possible, infrared imaging of the flight base heat shield and potentially of the plumes during SLS ascent will provide further corroboration of the flow physics model and ground test and optical diagnostic techniques developed.

EUS data analysis is currently ongoing and will support Block1B/EUS DAC2 design environments in months to come. OH-PLIF thermometry was performed for the first time in a launch vehicle base flow configuration to obtain a quantitative map of the base gas temperature. This temperature map will be compared with a spatially averaged data point obtained from tunable diode laser absorption spectroscopy. Another important assessment based on the new imaging data is the potential for localized RL10 and RS-25 nozzle heating due to stagnation shock impingement (Figures 7, 9 and 12).

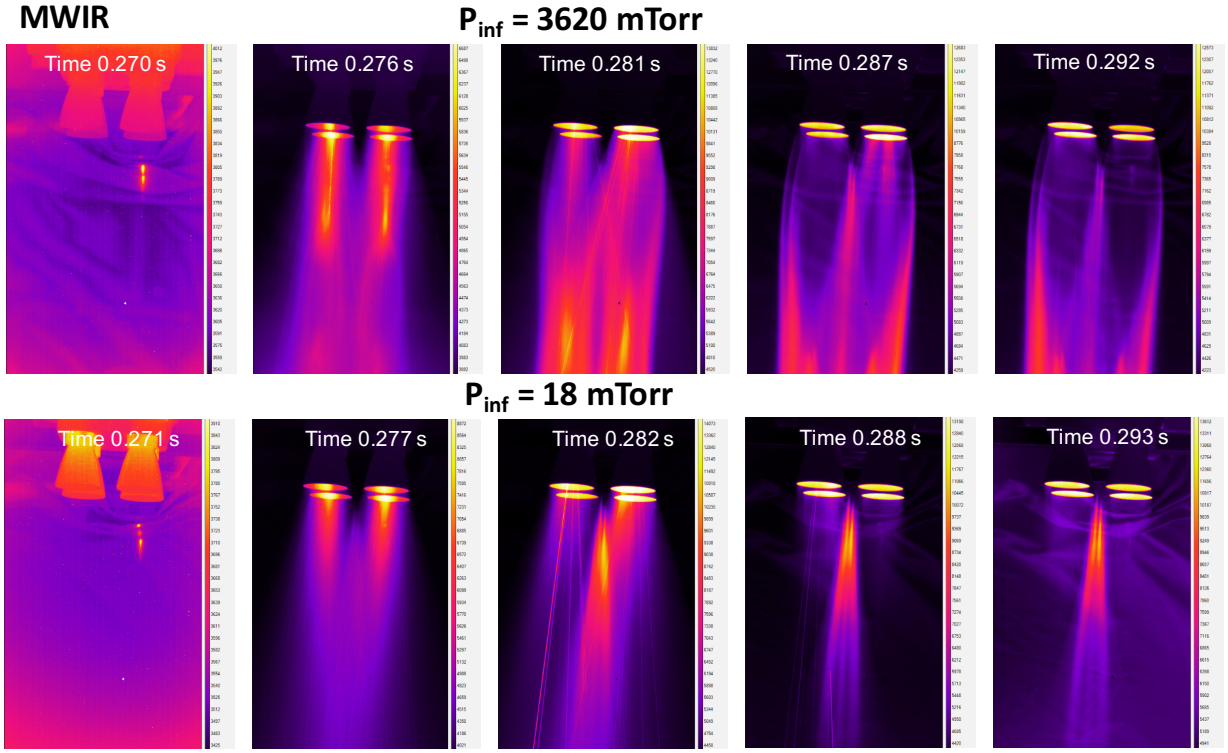

Figure 10. MWIR imaging time sequence of engine start-up at high P_{inf} (EUS Run 19) and low P_{inf} (EUS Run 16)

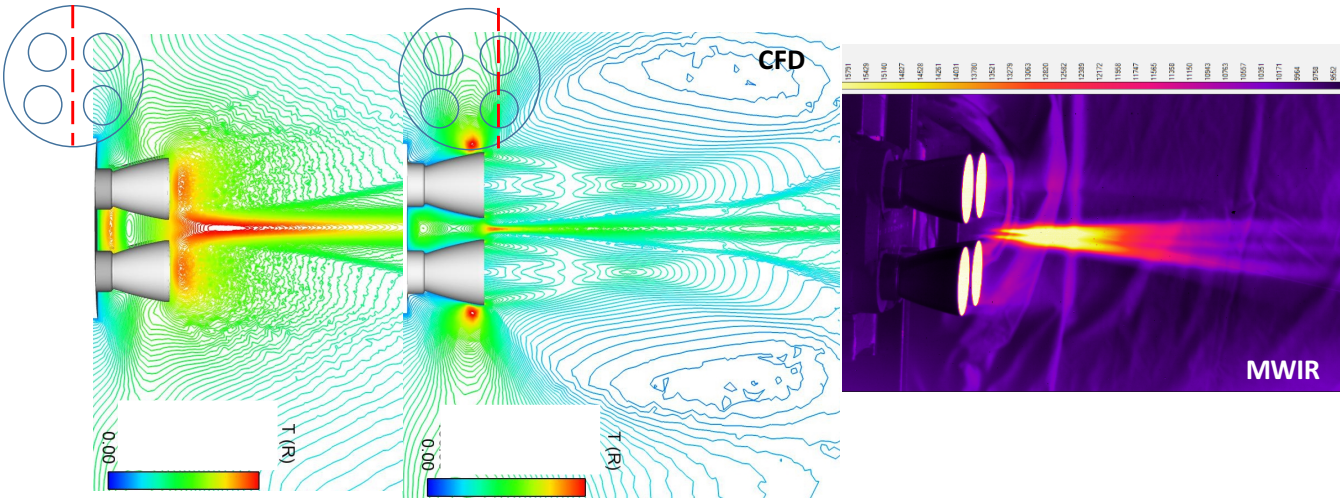

Figure 11. MWIR imaging captured EUS plume environments (EUS Run 6)

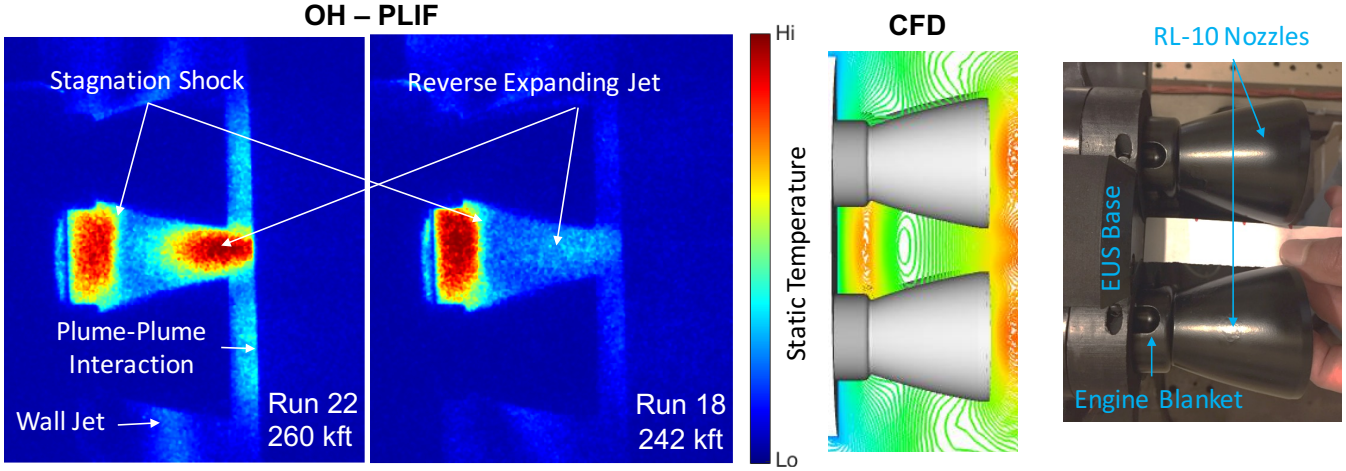

Figure 12. OH-PLIF BCL imaging captured EUS base flow environments

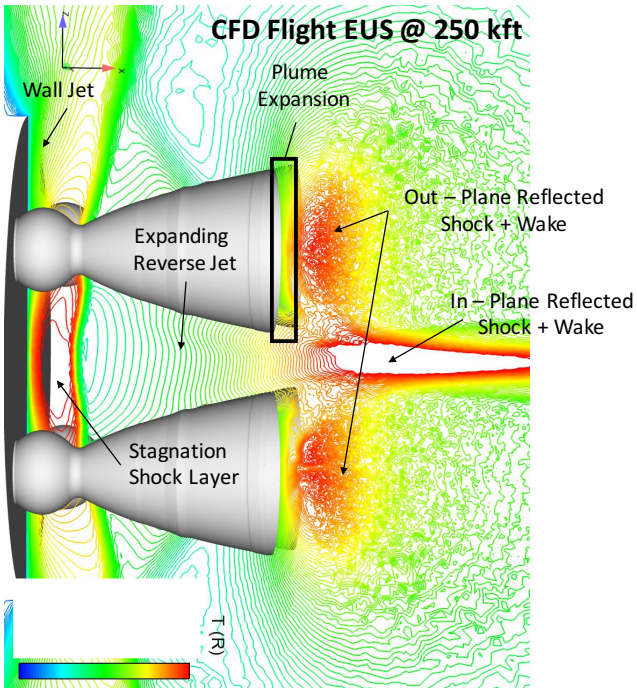

Figure 13. CFD BCL Plane of flight EUS base flow static temperature contours at 250 kft

C. Limitations

There are a few limitations that were observed from the current investigations. It should be noted that only one OH-PLIF image is acquired per short-duration test due to a 10 Hz pulse laser frequency. As a result, detailed statistics and dynamics of the base inviscid and turbulent flow structures are difficult to acquire during an engine burn. This leads to the inability to obtain dynamics information and larger uncertainty in flow field quantities. Another limitation is the small PLIF domain window which is not able to capture the entire base region. This is due to optimizing the required laser intensity within the sheet to obtain a good signal to noise image. As a result of the restricted funding, different angled PLIF sheets were not conducted which could provide further flow information. The biggest limitation is that since these test programs were short: on the scale of less than a week, in-depth technical investigation and data processing were not conducted to address certain diagnostic anomalies that occurred during testing.

IV. Conclusions and Forward Work

The TIP and EUS test programs have provided for the first time proof-of-concept and technical maturation that these diagnostic techniques are successful in visualizing and characterizing complex reacting plume-induced base flows. Details of the base flow structures have been successfully captured for the first time. As a result, we anticipate that these diagnostic techniques can visually capture plume-induced hot spots anywhere on the vehicle. Further and novel confirmation of the adequacy of short-duration propulsion ground test techniques were obtained with these non-intrusive diagnostics. This is the first time rocket plume-induced base flow visualization has been captured for reacting turbulent flows in a ground test, simulating launch vehicle ascent. However, in-depth characterization of base flow dynamics and unsteadiness will require further maturation of technologies. There are a number of forward work items needed to further mature these short-duration propulsion ground test technologies. These unique NASA-led test capabilities and these recent NASA test programs (supported by the TIP and EUS) have reduced their technical, cost and schedule risks.

NASA LaRC has obtained a 10 kHz pulse-burst laser system which could be enhanced to allow PLIF imaging. Together with a high speed intensifier, this system would have similar capability to that used in the present experiment except with 1000 times faster imaging acquisition speed. This will allow time-sequence movies to be obtained of the startup and establishment processes of rocket plume-induced flows for space vehicles for short-duration propulsion test technology, which can adequately capture both inviscid and turbulent flow characteristics. Furthermore, multiple images would provide statistics for uncertainty quantification. Another area to further mature is to maximize the PLIF sheet area while also obtaining high signal-to-noise ratio data. (In the data reported herein, subsequent processing showed that the laser fluence

was in the saturation regime and that the same fluorescence intensities could have been obtained even with a much larger laser sheet.) The third area is to image PLIF sheets at various planes, angles and orthogonal views to the plume-induced flows which will provide a more accurate assessment of all the "hot spots" in the region of interest. These areas were not formally investigated during these last few tests due to limited funding and a constrained schedule.

Although the project acquired high-speed IR images at 180 Hz for the FY16 TIP and EUS test programs, there were gaps in the image data during engine start-up, shut-down and steady engine burn. This prevented us from developing a high-quality integrated steady-state IR image. It would have been ideal to have a higher sampling speed IR camera which operates at 565 Hz at full-resolution. The over-arching goal would be the development of a relatively long test program (two weeks) with more optimized state-of-the-art diagnostics equipment to fully characterize plume-induced flows.

The FY16 TIP and EUS data is being used for the SLS base convection substantiation reports to confirm the ATA-002 SLS base environment data and to mitigate risk associated with short-duration propulsion wind-tunnel testing. Having both flow visualization and measurement data is important to verify and understand environments and to build confidence prior to obtaining DFI. This ground test technology and new optical diagnostic techniques at relatively low cost can also be adequately used to investigate NASA entry, descent and landing technologies such as supersonic retro-propulsion and landers during the descent phase.

Acknowledgements

Special thanks to Dr. Chong Lee and Dr. Francisco Canabal of EV33 for generating high-altitude computational solutions of the EUS flight & sub-scale model and SLS core-stage sub-scale model flow fields. Also thanks to Ross Burns of the National Institute of Aerospace, Hampton VA, who showed that the fluorescence intensity in not sensitive to the laser intensity, suggesting that the fluorescence was saturated to such an extent that the laser intensity correction was unnecessary.

References

[1] Bird, K.D., C.L. Mathis and J.W. Reece (1962), The application of short-duration techniques to the experimental study of base heating, CAL-Report No. HM-1510-1, Cornell Aeronautical Laboratory, Inc., Buffalo, NY

[2] Mehta, M., A.T. Dufrene, C.M. Seaford and K.S. Knox (2016), Space Launch System Base Heating Test: Environments and Base Flow Physics, AIAA 2016-0547, 54th AIAA SciTech Meeting, San Diego, CA

[3] Parker R., Z.R. Carr, A.T. Dufrene and M. Mehta (2016), Space Launch System Base Heating Test: Tunable Diode Laser Absorption Spectroscopy, AIAA 2016-0548, 54th AIAA SciTech Meeting, San Diego, CA

[4] Bender, R.L., T.F. Greenwood, Y.C Lee and R.L. Carter (1978), IH-39 Base Heating Test Data Analysis, NASA CR-NAS8-29270, NASA MSFC, AL

[5] Mullen, C.R., R.L. Bender, R.L. Bevill, J. Reardon and L. Hatley (1972), Saturn Base Heating Handbook, NASA CR-61390, NASA MSFC, AL

[6] Mehta, M., C.M. Seaford, B.C. Kovarik, A.T. Dufrene, N. Solly, R.D. Kirchner and C.D. Engel (2014), Space Launch System Base Heating Test: Sub-scale Rocket Engine/Motor Design, Development and Performance Analysis, AIAA 2014-1255, 52nd AIAA SciTech, National Harbor, MD

[7] J. A. Wilkes, D. W. Alderfer, S. B. Jones, and P. M. Danehy, "Portable Fluorescence Imaging System for Hypersonic Flow Facilities," *JANNAF Interagency Propulsion Committee Meeting*, Colorado Springs, Colorado, Dec. 2003.

[8] P. M. Danehy, J. A. Inman, D. W. Alderfer, G. M. Buck, B. Bathel, "Visualization of flowfield modification by RCS jets on a capsule entry vehicle", AIAA Paper 2008-1231, 46th AIAA Aerospace Sciences Meeting and Exhibit, Reno, Nevada, Jan. 7-10, 2008.

[9] P. M. Danehy, D. W. Alderfer, J. A. Inman, K. T. Berger, G. M. Buck, and R. J. Schwartz, "Fluorescence Imaging and Streamline Visualization of Hypersonic Flow Over Rapid Prototype Wind-Tunnel Models" Proc. IMechE, Part G: J. Aerospace Engineering, 222 (G5), pp. 637-651, 2008.

[10] D. W. Alderfer, P. M. Danehy, J. A. Wilkes Inman, K. T. Berger, G. M. Buck, and R. J. Schwartz, "Fluorescence Visualization of Hypersonic Flow Over Rapid Prototype Wind-Tunnel Models" AIAA Paper 2007-1063, 45th AIAA Aerospace Sciences Meeting and Exhibit, Reno, Nevada, Jan. 8-11, 2007.